

DP-DCAN: Differentially Private Deep Contrastive Autoencoder Network for Single-cell Clustering

Huifa Li^{1*}, Jie Fu^{1*}, Zhili Chen^{1(✉)}, Xiaomin Yang^{2(✉)}, Haitao Liu¹, and Xinpeng Ling¹

¹ Shanghai Key Laboratory of Trustworthy Computing, East China Normal University, Shanghai, China

{huifali, jie.fu, htliu, xpling}@stu.ecnu.edu.cn, zhlichen@sei.ecnu.edu.cn

² Xinhua Hospital, School of Medicine, Shanghai Jiao Tong University, Shanghai, China

yangxiaomin@xinhua.med.com.cn

Abstract. Single-cell RNA sequencing (scRNA-seq) is important to transcriptomic analysis of gene expression. Recently, deep learning has facilitated the analysis of high-dimensional single-cell data. Unfortunately, deep learning models may leak sensitive information about users. As a result, Differential Privacy (DP) is increasingly being used to protect privacy. However, existing DP methods usually perturb whole neural networks to achieve differential privacy, and hence result in great performance overheads. To address this challenge, in this paper, we take advantage of the uniqueness of the autoencoder that it outputs only the dimension-reduced vector in the middle of the network, and design a Differentially Private Deep Contrastive Autoencoder Network (DP-DCAN) by partial network perturbation for single-cell clustering. Firstly, we use contrastive learning to enhance the feature extraction of the autoencoder. And then, since only partial network is added with noise, the performance improvement is obvious and twofold: one part of network is trained with less noise due to a bigger privacy budget, and the other part is trained without any noise. Experimental results of 8 datasets have verified that DP-DCAN is superior to the traditional DP scheme with whole network perturbation.

Keywords: scRNA-seq data · Autoencoder · Differential privacy · Contrastive learning.

1 Introduction

Single-cell RNA sequencing (scRNA-seq) has enabled unbiased, high-throughput, and high-resolution transcriptome analysis at the level of individual cells [14, 49], playing a crucial role in identifying cell types through transcriptome analysis,

* : These authors contributed equally.

investigating developmental biology, uncovering intricate diseases and predicting cell developmental pathways. Therefore, the accurate identification of cell types is a crucial step in scRNA-seq analysis. Clustering is a very powerful method for cell type annotation, as it can identify cell types in an unbiased manner. However, the quality of feature representation has remained a bottleneck for the performance of clustering. Besides, scRNA-seq data associated with diseases are highly sensitive and need rigorous privacy protection [6].

In general, deep autoencoder is a type of neural network with the primary purpose of learning an informative representation of the data that can be used for different applications and has emerged as a powerful tool for clustering. In this work, we focus on scRNA-seq data clustering. In the setting of scRNA-seq data clustering, the dataset consists of multiple cells, and the autoencoder is trained to learn a useful representation for each cell. The representation is input to a classifier to predict a specific cell type. In recent years, many novel deep learning clustering approaches with autoencoder have successfully developed to model the high-dimensional and sparse scRNA-seq data, such as scDC [37], scDCC [38], bmVAE [44], DCA [13], scSemiCluster [8] and scVAE [17].

However, drawing meaningful insights in many of these approaches fundamentally relies upon the utilization of privacy-sensitive, often scarce, training data associated with individuals. scRNA-seq data yields some important privacy concerns, including genetic conditions [30] and predispositions to specific diseases [31]. In contrast to the modifiability of compromised credit card numbers, scRNA-seq data, once revealed, remain unchangeable. The revelation of these holds the potential to detrimentally affect patients by influencing their prospects in employment and education.

It is thus apparent that the implementation of privacy-enhancing techniques is required to facilitate the training of models of sensitive scRNA-seq data. One of the state-of-the-art paradigms to prevent privacy disclosure in machine learning is differential privacy (DP) [1, 15, 16, 27]. DP is a pioneering approach in the domain of privacy-preserving data analysis. It operates on the principle of introducing controlled noise into the data or its analysis results, which is carefully calibrated to protect individual privacy without significantly compromising the data’s utility for group-level inferences. Several studies have demonstrated that the implementation of differential privacy (DP) can effectively mitigate the inadvertent disclosure of private training data, including vulnerabilities to membership inference attacks [19, 24, 46] during the training process. Many applications of differential privacy in the fields of biology and medicine have been proposed [7, 39]. However, there is no differentially private learning methods have taken scRNA-seq data into account.

Unfortunately, the random noise introduced by differential privacy leads to poor performance of current differential privacy deep learning models [2]. Additionally, research indicates that the noise introduced by differential privacy increases as the model size grows [35]. Achieving good performance of trained models while ensuring differential privacy protection is a challenge, especially in autoencoders, as they are more sensitive to random noise [18].

In this paper, we first introduce a Differentially Private Deep Contrastive Autoencoder Network for single-cell dimension reduction and clustering (DP-DCAN). The algorithm leverages autoencoders to learn discriminative features of instances and utilizes contrastive learning to enhance the extraction of features by contrasting the similarity and dissimilarity of samples under different clusters. In addition, we incorporate differential privacy into the process to protect the privacy of clustering outputs. However, adding differential privacy protection at the autoencoder stage is non-trivial because the random noise introduced by differential privacy affects the training effectiveness of the autoencoder. Therefore, based on the post-processing property of differential privacy [52], we designed a differential privacy method with partial network perturbation that can effectively reduce the impact of noise on our autoencoder model. The experimental results demonstrated that our algorithm DP-DCAN can achieve excellent performance under differential privacy protection on real scRNA-seq datasets.

The main contributions of our work are summarized below:

- We proposed a DP-DCAN algorithm. To the best of our knowledge, this is the first article to propose the differential privacy framework for single-cell clustering.
- We designed a differential privacy method with the partially perturbed network for autoencoder and the method can efficiently mitigate the performance sacrifice of the autoencoder model.
- We conducted a rigorous privacy analysis on the proposed method based on Rényi differential privacy, proving that it meets differential privacy.
- Comprehensive empirical evaluation on 8 public datasets. The results confirm that DP-DCAN can achieve superior clustering performance under the protection of differential privacy.

The rest of the paper is organized as follows. Section 2 provides an overview of the related work. Section 3 introduces the preliminary knowledge. In Section 4, we present the details of our method. Privacy analysis is conducted in Section 5 and the experimental results are presented in Section 6. Finally, Section 7 is the conclusion.

2 Related Work

2.1 Single-cell RNA-seq Data Clustering

Clustering is an unsupervised method capable of accurately identifying single-cell types. Deep embedding clustering methods perform clustering and feature learning which can address the challenge of high heterogeneity and sparsity in scRNA-seq data.

In the past years, deep learning methods have been used and advanced to analyze scRNA-seq data. Eraslan et al. [13] introduce the ZINB-based autoencoder to capture the complexity and non-linearity in scRNA-seq data. In another work,

Tian et al. [37] leverage a deep autoencoder as an embedding method, which simultaneously learns feature representation and clustering via explicit modeling of scRNA-seq data generation. Tian et al. [38] convert prior knowledge into soft pairwise constraints and add them as additional terms into the loss function for optimization. Moreover, Wang et al. [41] and Yu et al. [48] aggregate cell-cell relationships and identify cell clusters based on deep graph convolutional networks.

2.2 Differential Privacy in Medicine and Bioinformatics

There are a few works that take into account scRNA-seq data in differentially private learning. Liu et al. [26] propose a definition of adaptive differential privacy of character and its mechanisms satisfying expected privacy-preserving and expected data utility. Wu et al. [42] makes use of the closed frequent pattern set to reduce redundant motifs of result sets and obtain accurate motifs results, satisfying ϵ -differential privacy. Islam et al. [21] propose a differential privacy-based DL framework to solve biological problems: breast cancer status (BCS) and cancer type (CT) classification, and drug sensitivity prediction. Yilmaz et al. [47] propose a mechanism that considers the correlations in data during data sharing, eliminates statistically unlikely data values beforehand, and adjusts the probability distributions for each shared data point accordingly. To the best of our knowledge, the problem of how to achieve differentially private learning with the scRNA-seq data has not been well-addressed.

3 Preliminaries

In this section, we introduce and formalize the theory to train deep autoencoder using the concept of differentially private stochastic gradient descent (DP-SGD).

3.1 Deep Autoencoder

This semi-supervised learning method can be implemented by deep autoencoder(DAE) [34]. The DAE is typically composed of two main components: an encoder network and a decoder network, corresponding to f_e and f_d .

In particular, the autoencoder learns a map from the input to itself through a pair of encoding and decoding phases:

$$\hat{X} = f_d(f_e(X)). \quad (1)$$

where X is the input data, f_e is an encoding map from the input layer to the hidden layer, f_d is a decoding map from the hidden layer to the output layer, and \hat{X} is the reconstruction of the input data. The idea is to train f_e and f_d to minimize the difference between X and \hat{X} .

3.2 Differential Privacy

Differential privacy is a mathematically rigorous framework that formally defines data privacy. It requires that a single entry in the input dataset cannot result in statistically significant changes in the output [10–12] if differential privacy holds.

Definition 1. ((ϵ, δ) -Differential Privacy). *The randomized mechanism A provides (ϵ, δ) -Differential Privacy (DP), if for any two neighboring datasets D and D' that differ in only a single entry, $\forall S \subseteq \text{Range}(A)$,*

$$\Pr(A(D) \in S) < e^\epsilon \times \Pr(A(D') \in S) + \delta. \quad (2)$$

Here, $\epsilon > 0$ controls the level of privacy guarantee in the worst case. The smaller ϵ is, the stronger the privacy level is. The factor $\delta > 0$ is the failure probability that the property does not hold. In practice, the value of δ should be negligible [32, 53], particularly less than $\frac{1}{|D|}$.

3.3 Differentially Private Stochastic Gradient Descent

Abadi et al. [1] proposed Differentially Private Stochastic Gradient Descent (DP-SGD) which is a widely adopted scheme for training deep neural networks with differential privacy guarantees. Specifically, in each iteration t , a batch of tuples \mathcal{B}_t is sampled from D with a fixed probability $\frac{b}{|D|}$, where b is batch size. After computing the gradient of each tuple $x_i \in \mathcal{B}_t$ as $g_t(x_i) = \nabla_{\theta_i} L(\theta_i, x_i)$, where θ_i is model parameter for the i -th sample, DPSGD clips each per-sample gradient according to a fixed ℓ_2 norm (3).

$$\begin{aligned} \bar{g}_t(x_i) &= \text{Clip}(g_t(x_i); C), \\ &= g_t(x_i) / \max\left(1, \frac{\|g_t(x_i)\|_2}{C}\right). \end{aligned} \quad (3)$$

In this way, for any two neighboring datasets, the sensitivity of the query $\sum_{i \in \mathcal{B}_t} g(x_i)$ is bounded by C . Then, it adds Gaussian noise scaling with this norm to the sum of the gradients when computing the batch-averaged gradients:

$$\tilde{g}_t = \frac{1}{b} \left(\sum_{i \in \mathcal{B}_t} \bar{g}_t(x_i) + \mathcal{N}(0, \sigma^2 C^2 \mathbf{I}) \right), \quad (4)$$

where σ is the noise scale depending on the privacy budget. Last, the gradient descent is performed based on the batch-averaged gradients. Since initial models are randomly generated and independent of the sample data, and the batch-averaged gradients satisfy the differential privacy, the resulting models also satisfy the differential privacy due to the post-processing property.

3.4 Privacy Threat Model

In the context of deep learning models for scRNA-seq data sharing as shown in Fig. 1, it is presumed that the patients and medical center are entities considered trustworthy. Conversely, the querying party, which utilizes the shared model, is assumed to be honest but curious. Therefore, the querying party is curious about sensitive information in scRNA-seq data analysis. Also, considering the querying party has full background knowledge of genome data. Patients send biological samples to the medical center, where scRNA-seq data can be obtained by sequencing. Therefore, the scRNA-seq data of the medical center is reliable. In the scRNA-seq data sharing model, the specific privacy threat model is as follows: The querying party is honest but curious; the querying party can obtain all background knowledge about patients’ scRNA-seq data; Patients, medical center, and querying party are rational.

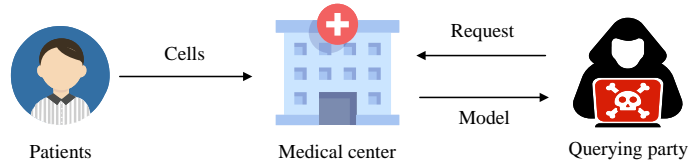


Fig. 1. Privacy threat model of scRNA-seq data deep learning.

4 Methodology

In this section, we first introduce the proposed method termed DP-DCAN. We then present our idea of a differentially private single-cell autoencoder network. And we introduce a contrastive learning module. Finally, we elaborate on the proposed loss function in DP-DCAN.

4.1 Overview

As shown in Fig. 2, our DP-DCAN framework mainly consists of two key components: the private single-cell autoencoder network and the two-stage contrastive learning module. In the private single-cell autoencoder network, the autoencoder is trained to learn the essential feature representation of the scRNA-seq data while preventing leakage of sensitive information elegantly. In the two-stage contrastive learning module, we further enhance the autoencoder’s understanding of feature representation by comparing the similarities and disparities between different samples and across various clusters.

The detailed procedure of DP-DCAN is outlined in Algorithm 1. The algorithm employs a two-stage training. In the first stage, the autoencoder maximizes

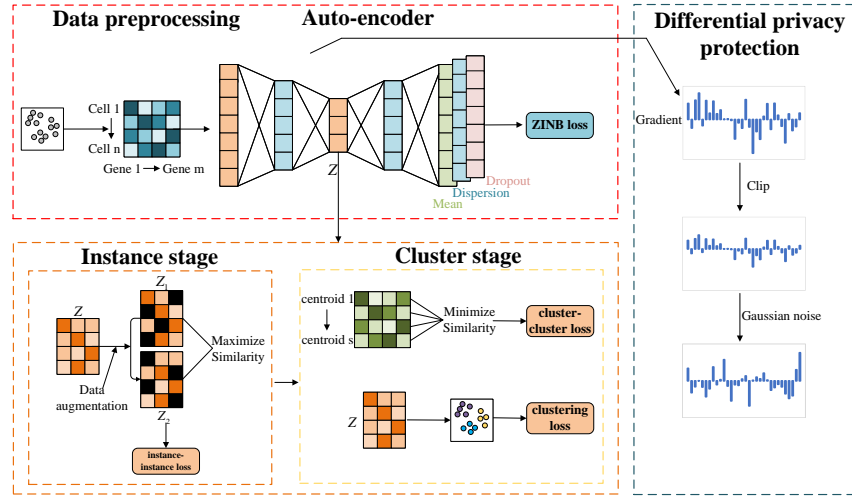


Fig. 2. The overview of DP-DCAN.

the similarity between instances from the same cluster in compressed feature space as shown in Lines 4-8. The second stage enables the autoencoder to maximize the distance between different clusters as shown in Lines 11-15. The design of loss functions $\mathcal{L}_{instance}$ and $\mathcal{L}_{cluster}$ for two-stage training is shown in Section 4.4. In the two stages, Gaussian noise is added to the encoder network θ_e of auto-encoder while optimizing the model in Lines 6 and 13. The decoder network θ_d of autoencoder doesn't be disturbed because it's useless during inference. Lines 7 and 14 keep track of the privacy loss of RDP and convert it to (ϵ, δ) in Line 16.

4.2 Differentially Private Single-cell Autoencoder Network

The trained encoder can map the high-dimensional to low-dimensional and the trained decoder doesn't work during inference. Moreover, the existing DP methods usually perturb whole neural networks to achieve differential privacy and hence result in great performance overheads. Inspired by these, We proposed a differentially private deep autoencoder network that only adds noise to the gradient of the encoder while minimizing the empirical loss function for single-cell clustering. The network is based on a Zero-Inflated Negative Binomial (ZINB) loss function that can learn the hidden feature representation of scRNA-seq data. Within this framework, fully connected layers stacked in both the encoder and decoder facilitate the capture of intricate representation embeddings from scRNA-seq datasets.

Algorithm 2 outlines our training approach with parameters θ by minimizing the empirical loss function $\mathcal{L}(\theta)$. The encoder parameters θ_e are perturbed

Algorithm 1 DP-DCAN framework

Input: Examples $X = \{x_1, x_2, \dots, x_N\}$, learning rate η , lot size L , noise scale σ , clipping bound C .**Output:** θ_e and privacy budget (ϵ, δ) .

- 1: Initialize autoencoder parameter $\theta = \{\theta_e, \theta_d\}$ randomly, $R_1=0, R_2 = 0$
 - 2: # Instance stage
 - 3: Design $\mathcal{L}_{instance}$ as shown in Equ. (10)
 - 4: **for** $t_1 \in [1, T_1]$ **do**
 - 5: $DPAN_{input} \leftarrow (\theta_e^{t_1}, \theta_d^{t_1}, \mathcal{L}_{instance}, X, L, C, \sigma, \eta)$
 - 6: $(\theta_e^{t_1+1}, \theta_d^{t_1+1}), R_1 \leftarrow DPAN(DPAN_{input})$
 - 7: $R_1+ = R_1$
 - 8: **end for**
 - 9: # Cluster stage
 - 10: Design $\mathcal{L}_{cluster}$ as shown in Equ. (14)
 - 11: **for** $t_2 \in [T_1 + 1, T_2]$ **do**
 - 12: $DPAN_{input} \leftarrow (\theta_e^{t_2}, \theta_d^{t_2}, \mathcal{L}_{cluster}, X, L, C, \sigma, \eta)$
 - 13: $(\theta_e^{t_2+1}, \theta_d^{t_2+1}), R_2 \leftarrow DPAN(DPAN_{input})$
 - 14: $R_2+ = R_2$
 - 15: **end for**
 - 16: Compute privacy budget ϵ by Theorem 1
 - 17: **return** $\theta_e^{T_2}$ and (ϵ, δ) .
-

when optimizing. And the decoder parameters θ_d don't be perturbed. At each optimization step, we compute the gradient $g(x_i)$ including protected gradient $g_e(x_i)$ and exposed parameters $g_d(x_i)$ for a random subset of samples, clip the ℓ_2 norm of each gradient and compute the average in Lines 1-5. Then, we add noise to the gradient of θ_e in order to protect privacy with the smallest possible performance loss and take a step in the opposite direction of this average noisy gradient in Lines 7-10. At the end, we compute the privacy budget by Theorem 2 in Line 11. The privacy analysis is in Section 5.

4.3 Contrastive Learning Module

To capture the relationships between cells, We integrated a two-stage contrastive learning module into our model to enhance the autoencoder's ability to discern more discriminative features within instances without negative pairs and clusters. In the first stage, specific samples x are augmented into $\{x_1, x_2\}$ as positive examples. Then, the augmented data is mapped to a lower-dimensional space using the encoder. Inspired by SimSiam [9], which does not rely on negative pairs. We maximize the similarity between two augmentations of x in order to converge towards improved performance. This approach learns more robust and useful representations by enhancing the similarity of samples from the same class. Instance-level contrastive learning extracts distinctive features by minimizing differences between these instances. We minimize their negative cosine

Algorithm 2 Differentially private autoencoder network (DPAN)

Input: Examples x_1, x_2, \dots, x_N , learning rate η , lot size L , loss function $\mathcal{L}(\theta)$, noise scale σ , clipping bound C .

Output: $(\hat{\theta}_e, \hat{\theta}_d)$ and privacy budget RDP .

- 1: Take a random sample \mathcal{B} with probability L/N
- 2: **for** $x_i \in \mathcal{B}$ **do**
- 3: Compute $g_e(x_i), g_d(x_i) \leftarrow \nabla_{\theta} \mathcal{L}(\theta, x_i)$
- 4: $\bar{g}_e(x_i) \leftarrow g_e(x_i) / \max(1, \frac{\|g_e(x_i)\|_2}{C})$
- 5: $\bar{g}_d(x_i) \leftarrow g_d(x_i) / \max(1, \frac{\|g_d(x_i)\|_2}{C})$
- 6: **end for**
- 7: $\tilde{g}_e \leftarrow \frac{1}{L} (\sum_i^L \bar{g}_e(x_i) + \mathcal{N}(0, \sigma^2 C^2 \mathbf{I}))$
- 8: $\tilde{g}_d \leftarrow \frac{1}{L} \sum_i^L \bar{g}_d(x_i)$
- 9: $\hat{\theta}_e \leftarrow \theta_e - \eta \tilde{g}_e$
- 10: $\hat{\theta}_d \leftarrow \theta_d - \eta \tilde{g}_d$
- 11: Compute privacy budget RDP by Theorem 2
- 12: **return** $(\hat{\theta}_e, \hat{\theta}_d), RDP$.

similarity:

$$\mathcal{L}_{ii} = -\frac{z_1}{\|z_1\|_2} \cdot \frac{z_2}{\|z_2\|_2}. \quad (5)$$

where z_1, z_2 are x_1, x_2 which are mapped to a low dimensional vector through an encoder, and $\|\cdot\|$ is ℓ_2 -norm.

In the second stage, based on the centroids as representative positions for each cluster, cluster-level contrastive learning is applied to capture discriminative cluster features. Utilizing K-means, we acquire centroid positions. Cluster-level contrastive learning is committed to maximizing the distance between clusters, ensuring clusters are positioned as distantly from each other as feasible:

$$\mathcal{L}_{cc} = \frac{1}{s^2} \sum_{i=0}^s \sum_{j=0}^s \frac{c_i}{\|c_i\|_2} \cdot \frac{c_j}{\|c_j\|_2}. \quad (6)$$

where c_i is the centroid of cluster i , c_j is the centroid of cluster j and s is the number of clusters.

4.4 Joint Embedding and Clustering Optimization

We use a hybrid loss to optimize our proposed DP-DCAN during the two-stage training phase. Different from the two-stage training proposed by Wang [40] that can't compute the gradient for each individual sample in a batch which is not suitable for differential privacy, our method is designed to calculate the gradient by an individual sample. Specifically, in the first stage, we jointly combined the reconstruction loss and the instance-instance loss to minimize the distance of the instances of the same cluster. Reconstruction loss $\mathcal{L}_{z_{inb}}$, instance-instance

loss \mathcal{L}_{ii} and hybrid loss $\mathcal{L}_{instance}$ are defined as follows:

$$\text{ZINB}(x|\pi, \mu, \theta) = \pi\delta_0(x) + (1 - \pi)\text{NB}(x|\mu, \theta), \quad (7)$$

$$\text{NB}(x|\mu, \theta) = \frac{\Gamma(x + \theta)}{x!\Gamma(\theta)} \left(\frac{\theta}{\theta + \mu}\right)^\theta \left(\frac{\mu}{\theta + \mu}\right)^x, \quad (8)$$

$$\mathcal{L}_{zinb}(X, \hat{X}) = -\log(\text{ZINB}(x|\pi, \mu, \theta)), \quad (9)$$

$$\mathcal{L}_{instance} = \rho\mathcal{L}_{zinb} + (1 - \rho)\mathcal{L}_{ii}. \quad (10)$$

where x is the expression value in cell, π is the probability of a dropout event, μ is the mean, and θ represents the divergence of the negative binomial distribution. ρ is a weighted factor that balance the impact of \mathcal{L}_{zinb} and \mathcal{L}_{ii} .

In the second stage, we employ reconstruction loss, clustering loss, and cluster-cluster loss to maximize the distance between clusters. Clustering loss represents the disparity between the clustering results and the true data distribution which is measured by Kullback–Leibler (KL) divergence [23]. Clustering loss \mathcal{L}_{cls} , cluster-cluster loss \mathcal{L}_{cc} and hybrid loss $\mathcal{L}_{cluster}$ are defined as follows:

$$q_{ij} = \frac{\left(1 + \|z_i - \lambda_j\|^2\right)^{-1}}{\sum_{j'} \left(1 + \|z_i - \lambda_{j'}\|^2\right)^{-1}}, \quad (11)$$

$$p_{ij} = \frac{q_{ij}^2 / \sum_j q_{ij}}{\sum_{j'} \left(q_{ij'}^2 / \sum_{j'} q_{ij'}\right)}, \quad (12)$$

$$L_{cls} = KL(P||Q) = \sum_i \sum_j p_{ij} \log \frac{p_{ij}}{q_{ij}}, \quad (13)$$

$$\mathcal{L}_{cluster} = \beta_1\mathcal{L}_{zinb} + \beta_2\mathcal{L}_{cls} + \beta_3\mathcal{L}_{cc}. \quad (14)$$

where q_{ij} is the soft label of the embedding point z_i . This label measures the similarity between z_i and cluster center λ_j by Student's t-distribution. The target distribution p_{ij} is obtained by squaring q_{ij} and then normalizing by the sum of the squared values across all clusters. β_1 , β_2 and β_3 are three weighted factors that balance the impact of \mathcal{L}_{zinb} , \mathcal{L}_{cls} and \mathcal{L}_{cc} . Their combined sum equals 1.

5 Privacy Analysis

Due to the latent representation being generated in the middle of the auto-encoder during inference, we just need to implement differential privacy on the encoder to achieve privacy protection according to the post-processing property of differential privacy [52]. The privacy guarantee of DP-DCAN is proved as follows:

Theorem 1. (Privacy loss of DP-DCAN). *The privacy loss of DP-DCAN satisfies:*

$$\begin{aligned} (\epsilon, \delta) = & (R1 + R2 + \log((\alpha - 1)/\alpha) \\ & - (\log \delta + \log \alpha)/(\alpha - 1), \delta). \end{aligned} \quad (15)$$

where $0 < \delta < 1$, R_1 and R_2 is the RDP of algorithm DPAN which is computed by Theorems 2.

Definition 2. (Composition of RDP [27]). For two randomized mechanisms f, g such that f is (α, R_1) -RDP and g is (α, R_2) -RDP the composition of f and g which is defined as (X, Y) (a sequence of results), where $X \sim f$ and $Y \sim g$, satisfies $(\alpha, R_1 + R_2)$ -RDP.

Definition 3. (Conversion from RDP to DP [3]). if a randomized mechanism $f : D \rightarrow \mathbb{R}$ satisfies (α, ϵ) -RDP, then it satisfies $(\epsilon + \log((\alpha - 1)/\alpha) - (\log \delta + \log \alpha)/(\alpha - 1), \delta)$ -DP for any $0 < \delta < 1$.

From Definition 2 and Definition 3, Theorem 1 is proofed.

Theorem 2. After T times of iterations, the RDP of training in DPAN satisfies:

$$R_{\text{train}}(\alpha) = \frac{T}{\alpha - 1} \ln \left[\sum_{i=0}^{\alpha} \binom{\alpha}{i} (1 - q)^{\alpha - i} q^i \exp \left(\frac{i^2 - i}{2\sigma^2} \right) \right]. \quad (16)$$

where $q = \frac{L}{N}$, σ is noise scale of training, and $\alpha > 1$ is the order.

Definitions 4 and 5 define Sampled Gaussian Mechanism (SGM) and Rényi Differential Privacy (RDP), respectively.

Definition 4. (Sampled Gaussian Mechanism (SGM) [28]). Let f be a function mapping subsets of S to \mathbb{R}^d . We define the Sampled Gaussian Mechanism (SGM) parameterized with the sampling rate $0 < q \leq 1$ and the $\sigma > 0$ as

$$SG_{q,\sigma}(S) \triangleq f(\{x : x \in S \text{ is sampled with probability } q\}) + \mathcal{N}(0, \sigma^2 \mathbb{I}^d). \quad (17)$$

In DPAN, f is the clipped gradient evaluation on sampled data points $f(\{x_i\}_{i \in B}) = \sum_{i \in B} \bar{g}_t(x_i)$. If \bar{g}_t is obtained by clipping g_t with a gradient norm bound C , then the sensitivity of f is equal to C .

Definition 5. (RDP privacy budget of SGM [28]). Let $SG_{q,\sigma}$, be the Sampled Gaussian Mechanism for some function f . If f has sensitivity 1, $SG_{q,\sigma}$ satisfies (α, R) -RDP whenever

$$R \leq \frac{1}{\alpha - 1} \log \max(A_\alpha(q, \sigma), B_\alpha(q, \sigma)). \quad (18)$$

where

$$\begin{cases} A_\alpha(q, \sigma) \triangleq \mathbb{E}_{z \sim \mu_0} [(\mu(z)/\mu_0(z))^\alpha], \\ B_\alpha(q, \sigma) \triangleq \mathbb{E}_{z \sim \mu} [(\mu_0(z)/\mu(z))^\alpha]. \end{cases} \quad (19)$$

with $\mu_0 \triangleq \mathcal{N}(0, \sigma^2)$, $\mu_1 \triangleq \mathcal{N}(1, \sigma^2)$ and $\mu \triangleq (1 - q)\mu_0 + q\mu_1$

Further, it holds $\forall (q, \sigma) \in (0, 1], \mathbb{R}^{+*}$, $A_\alpha(q, \sigma) \geq B_\alpha(q, \sigma)$. Thus, $SG_{q,\sigma}$ satisfies $(\alpha, \frac{1}{\alpha - 1} \log(A_\alpha(q, \sigma)))$ -RDP.

Finally, [28] describes a procedure to compute $A_\alpha(q, \sigma)$ depending on integer α .

$$A_\alpha = \sum_{k=0}^{\alpha} \binom{\alpha}{k} (1-q)^{\alpha-k} q^k \exp\left(\frac{k^2 - k}{2\sigma^2}\right) \quad (20)$$

From Definitions 4 and Definition 5, the Theorem 2 is proved.

6 EXPERIMENTS

Using differential privacy with partial perturbation can protect data privacy during the process of feature construction. In this section, we will explore the impact of the scope and intensity of model perturbation on model performance through a clustering task on multiple real-world scRNA-seq datasets.

6.1 Datasets and Pre-processing

1) *Dataset*: We conduct extensive experiments on 8 real-world scRNA-seq datasets from various sequencing platforms. The detailed information is described in Table 1. All 8 datasets are from different species, including mouse and human, as well as from different organs, such as the brain and embryo. Specifically, the numbers of cells range from 56 to 4271, and genes range from 3840 to 57241.

Table 1. The characteristics of the real scRNA-seq datasets

| Dataset | Cells | Genes | Class | Platform | Reference |
|---------|-------|-------|-------|-------------|-----------|
| Biase | 56 | 25737 | 5 | Smart-Seq | [5] |
| Yan | 124 | 3840 | 8 | Tang | [45] |
| Li | 561 | 57241 | 9 | SMARTer | [25] |
| Muraro | 2122 | 18915 | 9 | CEL-Seq2 | [29] |
| Klein | 2717 | 24175 | 4 | InDrop | [22] |
| Romanov | 2881 | 24352 | 7 | Unknown | [33] |
| Zeisel | 3005 | 19072 | 9 | Fluidigm C1 | [50] |
| Zheng | 4271 | 16449 | 8 | 10X | [51] |

2) *Pre-processing*: We adopt the scRNA-seq gene expression matrix X with n samples as the input. First, we filter the genes that have almost no expression value since there is a large amount of technical and biological noise in the stochastic single-cell gene expression pattern. Second, size factors are calculated by dividing the median expression value of each cell by the overall dataset median. The last step is to normalize the expression matrix, ensuring a variance of 1 and adjusting the mean to 0. After normalization, 2000 highly variable genes were selected as representative genes for each cell by scanpy package.

6.2 Implementation and Parameters Setting

In the proposed DP-DCAN framework, the sizes of the hidden fully connected layer in the encoder are set to (256, 64), the decoder is the reverse of the encoder, and the bottleneck layer (the latent space) has a size of 32. In our two-stage training process, the optimizer for the instance stage is Adam optimizer with setting $lr = 0.001$ and for the cluster stage is Adadelta with setting $lr = 1.0$. We set the batch size to around 0.1 of the dataset size. To achieve an appropriate trade-off between utility and privacy, the clipping bound $C = 0.1$ and $\delta = 10^{-5}$. Clustering performance is measured using metrics such as Normalized Mutual Information (NMI) [36] and Adjusted Rand Index (ARI) [20].

6.3 Experimental Evaluation

We evaluate the clustering performance on 8 scRNA-seq datasets in terms of both clustering methods (CL) and differential privacy algorithms (DP-ALG) shown in Table 2 and 3. DCAN represents our proposed deep contrastive learning autoencoder network for clustering, and the combination of our proposed privacy-preserving algorithm DPAN is DP-DCAN. To explore the ability of our proposed clustering method to extract features from cells, we compare DP-DCAN with two baseline methods for single-cell clustering, scDC and bmVAE both methods use an autoencoder as a tool for feature extraction. For our proposed differential privacy method DPAN, we demonstrate its superiority by comparing it with DP-PSAC [43], which is a differentially private per-sample adaptive clipping algorithm based on a non-monotonic adaptive weight function. Each clustering method was run ten times to take the average. The values of the best performance metrics are bolded.

Table 2. Performance of our method and the other clustering baseline methods on 8 scRNA-seq datasets when $\epsilon=8.0$.

| Metric | DP-ALG | CL | Biase | Yan | Li | Muraro | Klein | Romanov | Zeisel | Zhang |
|--------|-------------|-------|---------------|--------------|--------------|--------------|--------------|--------------|--------------|--------------|
| NMI | Non-private | scDC | 96.52 | 39.91 | 92.00 | 88.71 | 90.25 | 66.62 | 76.29 | 77.23 |
| | | bmVAE | 61.74 | 00.00 | 82.07 | 72.81 | 60.84 | 51.50 | 61.66 | 60.17 |
| | | DCAN | 100.00 | 84.35 | 91.22 | 90.22 | 95.76 | 61.54 | 69.13 | 76.34 |
| | DPAN | scDC | 63.60 | 30.14 | 88.14 | 82.73 | 93.28 | 62.67 | 71.89 | 75.48 |
| | | bmVAE | 00.00 | 30.28 | 68.13 | 64.06 | 61.82 | 52.34 | 45.44 | 62.97 |
| | | DCAN | 89.53 | 79.56 | 91.19 | 83.54 | 85.66 | 62.98 | 74.35 | 72.53 |
| ARI | Non-private | scDC | 98.21 | 19.66 | 80.16 | 92.55 | 86.65 | 63.75 | 72.90 | 73.72 |
| | | bmVAE | 34.91 | 00.00 | 69.55 | 49.06 | 37.24 | 25.22 | 32.19 | 30.43 |
| | | DCAN | 100.00 | 80.92 | 89.91 | 93.88 | 97.58 | 61.57 | 74.66 | 74.48 |
| | DPAN | scDC | 49.46 | 09.76 | 77.08 | 86.67 | 95.85 | 55.77 | 56.12 | 70.25 |
| | | bmVAE | 00.00 | 15.61 | 53.16 | 57.22 | 51.12 | 61.32 | 44.47 | 50.42 |
| | | DCAN | 93.40 | 68.19 | 90.27 | 88.58 | 81.18 | 68.72 | 74.17 | 70.87 |

Clustering Methods Evaluation. Table 2 summarizes the clustering performance of the proposed DCAN and the baseline clustering methods on 8 scRNA-seq datasets. In the non-private clustering methods, DCAN achieves the best NMI and ARI on 4 and 6 of 8 scRNA-seq datasets, respectively. In the private clustering methods, DCAN achieves the best NMI and ARI on 6 and 7 of 8 scRNA-seq datasets, respectively. The non-private clustering methods tend to achieve better NMI and ARI on most scRNA-seq datasets than private clustering methods. This is because differential privacy algorithms introduce noise into the model preventing the model from optimizing in the true direction. However, appropriate noise may result in performance gains. For example, in the Li and Romanov dataset, the NMI and ARI of DCAN with DPAN are better than those without DPAN. This phenomenon could be attributed to the introduction of moderate noise, which potentially enhances the generalization performance of the model, and additional investigation is warranted to fully comprehend this effect. Meanwhile, we can observe that bmVAE the clustering performance is not stable. The main reason is that further simulation of the data by ZINB distribution is necessary. Furthermore, the clustering performance of deep embedded clustering with the contrastive learning module is better and more stable, which again proves the superiority of DCAN.

Table 3. Performance of our method and the other differential privacy baseline method on 8 scRNA-seq datasets when $\epsilon=8.0$.

| Metric | CL | DP-ALG | Biase | Yan | Li | Muraro | Klein | Romanov | Zeisel | Zhang |
|--------|-------|---------|--------------|--------------|--------------|--------------|--------------|--------------|--------------|--------------|
| NMI | scDC | DP-PSAC | 32.13 | 29.33 | 36.60 | 51.53 | 61.87 | 29.69 | 45.21 | 33.46 |
| | | DPAN | 63.60 | 30.14 | 88.14 | 82.73 | 93.28 | 62.67 | 71.89 | 75.48 |
| | bmVAE | DP-PSAC | 00.00 | 00.00 | 00.00 | 56.99 | 41.19 | 43.45 | 47.24 | 41.87 |
| | | DPAN | 00.00 | 30.28 | 68.13 | 64.06 | 61.82 | 52.34 | 45.44 | 62.97 |
| | DCAN | DP-PSAC | 84.86 | 76.74 | 87.63 | 66.96 | 57.43 | 51.47 | 53.39 | 58.93 |
| | | DPAN | 89.53 | 79.56 | 91.19 | 83.54 | 85.66 | 62.98 | 74.35 | 72.53 |
| ARI | scDC | DP-PSAC | 23.44 | 11.98 | 16.86 | 40.08 | 59.11 | 37.95 | 33.17 | 23.90 |
| | | DPAN | 49.46 | 09.76 | 77.08 | 86.67 | 95.85 | 55.77 | 56.12 | 70.25 |
| | bmVAE | DP-PSAC | 00.00 | 00.00 | 00.00 | 54.69 | 45.66 | 58.54 | 41.23 | 34.60 |
| | | DPAN | 00.00 | 15.61 | 53.16 | 57.22 | 51.12 | 61.32 | 44.47 | 50.42 |
| | DCAN | DP-PSAC | 78.70 | 62.59 | 78.28 | 70.33 | 45.40 | 61.40 | 62.21 | 47.62 |
| | | DPAN | 93.40 | 68.19 | 90.27 | 88.58 | 81.18 | 68.72 | 74.17 | 70.87 |

Differential Privacy Methods Evaluation. Table 3 shows the impact of various differential privacy algorithms on the performance of different clustering methods. We can observe that our DPAN outperforms the other baseline differential privacy algorithm for clustering performance. For the 8 scRNA-seq

datasets, the clustering methods with DPAN achieve the best NMI and ARI on more than 6 of these datasets, respectively. This is because the DPAN is able to mitigate the loss of performance by centrally allocating the privacy budget to the encoder part of the model. In clustering methods scDC and bmVAE, DPAN significantly maintains the ability of the model to learn the feature representation of the data, while DP-PSAC exhibits a tendency to excessively disrupt the model. Even DP-PSAC has repeatedly shown ARI and NMI values are equal 0, indicating a loss of the ability to effectively extract model features. In the proposed clustering method DCAN with DPAN has achieved the best performance across all datasets compared with DP-PSAC. In summary, we can conclude that DP-DCAN performs better than the other methods under two clustering evaluation metrics. To demonstrate the intuitive discrimination ability of DP-DCAN, we employ the Uniform Manifold Approximation and Projection (UMAP) [4] technique with default parameters to project the scRNA-seq data into a 2D space on the Muraro datasets in Fig. 3.

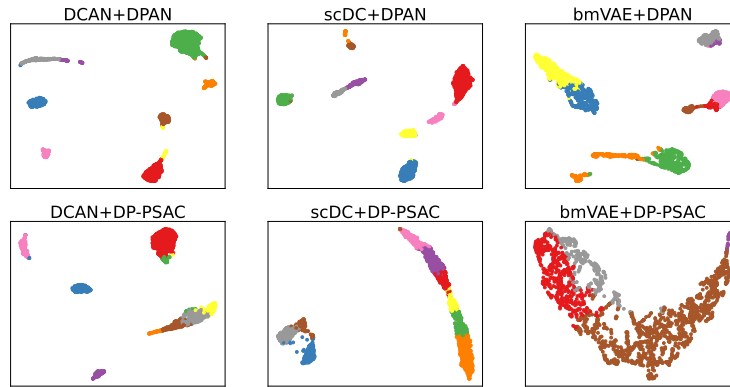


Fig. 3. Comparison of clustering results with 2D visualization by UMAP on the Muraro dataset.

6.4 Partial Network Perturbation vs. Entire Network Perturbation

We conducted a comparative analysis of the proposed DP-DCAN and DPE-DCAN, the latter involving perturbation of the entire model during the training process.

Fig. 4 shows the clustering performance of our method against DPE-DCAN when the same noise scale $\sigma = 2.00$. For each scRNA-seq dataset, we observe that the DP-DCAN generally outperforms the DPE-DCAN. On average, the NMI and ARI scores of DP-DCAN are more than 6.32% and 9.82% higher than the scores of the DPE-DCAN, respectively. This is because, with the same noise scale, DP-DCAN solely introduces perturbations to the model’s encoder, while

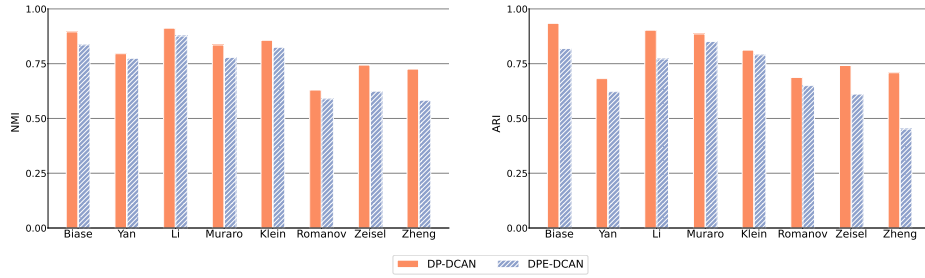


Fig. 4. Clustering performance of DP-DCAN and DPE-DCAN when $\sigma = 2.00$.

DPE-DCAN necessitates perturbing the entire model. Therefore, during training, DP-DCAN demonstrates superior convergence in the model training process. Additionally, the privacy budget of DP-DCAN, with $\epsilon = 8.0$, is smaller than the privacy budget of DPE-DCAN, with $\epsilon = 12.0$ at the same noise intensity. In conclusion, this experiment provides intuitive evidence to confirm that DP-DCAN can provide reliable and remarkable performance, even with a lower privacy budget.

As depicted in Fig. 5, we compare the proposed DP-DCAN and DPE-DCAN when the $\epsilon = 8.0$. Obviously, DP-DCAN outperforms the DPE-DCAN for clustering performance for all scRNA-seq datasets. Even in the Klein dataset, the NMI and ARI scores of DP-DCAN are 25.25% and 33.35% higher than DPE-DCAN, respectively, indicating a significant performance gap. This finding underscores the importance of partial network perturbation. In the context of a designated privacy allocation, enhancing the safeguarding of the model’s architecture necessitates the incorporation of increased perturbation within the gradients. Notably, the noise scale for DP-DCAN stands at 2.00, while for DPE-DCAN, it is set to 4.36. Considering the collective impact of noise intensity and the scope of noise impact, our method, DP-DCAN, employing a partially perturbed network, has exhibited exceptional efficacy across various scRNA-seq datasets.

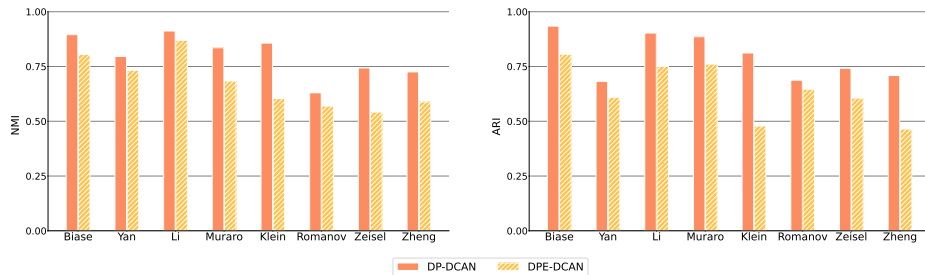


Fig. 5. Clustering performance of DP-DCAN and DPE-DCAN when $\epsilon = 8.0$.

6.5 Unveiling Model Perturbation

In an autoencoder network, the hidden fully connected layer can provide the functionality of feature learning and data reconstruction. To explore the impact of the scope of the perturbed layer, we apply DP-DCAN on real scRNA-seq datasets with perturbed layers from 1 to 6 with the noise scale $\sigma = 2.00$. Table 4 tabulates the average NMI and ARI values on the 8 scRNA-seq datasets for the 6 cases with DP-DCAN. As shown in Table 4, it can be clearly observed that clustering performance exhibits a fluctuating pattern with perturbed layers from 1 to 6. The superior performance of $layer_1$ can be ascribed to its inherent role in extracting fundamental features from the input data. Consequently, the introduction of noise to the gradients of the first layer during training may serve to augment the model’s generalization capability. The diminished performance observed for $layer_{1-2}$ in comparison to $layer_1$ could potentially be attributed to the second layer’s specific task of capturing more intricate features, rendering it more susceptible to the impact of noise. The improved performance noted for $layer_{1-3}$ and $layer_{1-4}$ in contrast to $layer_{1-2}$ may be ascribed to the equilibrium achieved through the introduction of noise during the model’s training process. The decline in performance for $layer_{1-5}$ and $layer_{1-6}$ may be attributed to the broader spectrum of noise influencing these layers, consequently leading to a deterioration in overall model performance.

Table 4. Clustering performance of DP-DCAN under different perturbation scopes.

| Metric | $layer_1$ | $layer_{1-2}$ | $layer_{1-3}$ | $layer_{1-4}$ | $layer_{1-5}$ | $layer_{1-6}$ |
|--------|-----------|---------------|---------------|---------------|---------------|---------------|
| NMI | 81.29 | 76.47 | 79.91 | 81.09 | 80.49 | 73.60 |
| ARI | 78.76 | 72.92 | 79.42 | 79.49 | 76.88 | 69.60 |

6.6 Differential Privacy Budget Analysis

Table 5 shows the clustering performance of our method at different noise levels. In this experiment, we vary the privacy budget $\epsilon \in \{4.0, 6.0, 8.0\}$ on 8 scRNA-seq datasets. As depicted in Table 5, we observe that as the privacy budget (privacy protection level) decreases, there is a general trend of decreasing NMI and ARI across the datasets. However, in the Biase dataset, the NMI and ARI violate this trend. Maybe this can be attributed to the introduction of moderate noise. Therefore, there is a trade-off between privacy protection and performance. This is a crucial result since smaller privacy budget values enforce stronger privacy guarantees. In cases where the privacy budget assumes larger values, such as privacy budget = 4.0, 6.0, 8.0, indicating the introduction of minimal noise into the model, the efficiencies of the model tend to converge towards heightened prediction accuracies. Balancing the privacy budget in differential privacy with model performance is a nuanced process that requires careful consideration of

the privacy requirements, the sensitivity of the data, and the acceptable level of accuracy for the model’s application. Moreover, DP-DCAN demonstrates strong robustness to different noise levels.

Table 5. Clustering performance of DP-DCAN on different privacy budgets.

| Metric | ϵ | σ | Biase | Yan | Li | Muraro | Klein | Romanov | Zeisel | Zheng |
|--------|------------|----------|-------|-------|-------|--------|-------|---------|--------|-------|
| NMI | 8.0 | 2.00 | 89.53 | 79.56 | 91.19 | 83.54 | 85.66 | 62.98 | 74.35 | 72.53 |
| | 6.0 | 2.49 | 96.52 | 77.49 | 90.62 | 83.47 | 85.61 | 62.13 | 74.48 | 72.53 |
| | 4.0 | 3.46 | 92.41 | 72.10 | 90.58 | 82.80 | 85.30 | 61.73 | 74.91 | 67.93 |
| ARI | 8.0 | 2.00 | 93.40 | 68.19 | 90.27 | 88.58 | 81.18 | 68.72 | 74.17 | 70.87 |
| | 6.0 | 2.49 | 98.21 | 69.42 | 89.28 | 88.41 | 81.10 | 68.23 | 75.09 | 68.12 |
| | 4.0 | 3.46 | 94.39 | 57.58 | 88.45 | 87.71 | 80.84 | 68.12 | 75.67 | 59.78 |

7 Conclusion

In this work, We propose DP-DCAN, a differentially private deep contrastive autoencoder network for single-cell clustering. Our scheme utilizes contrastive learning to enhance the feature extraction of the autoencoder. To protect single-cell privacy, we incorporate differential privacy for autoencoder during training. Furthermore, we design the partial network perturbation method for autoencoder. This perturbation method reduces the model dimension of the perturbation and ensures the utility. We conduct a comprehensive privacy analysis of our approach using RDP and validate our scheme through extensive experiments. The results indicate that DP-DCAN can achieve excellent performance under differential privacy protection. In future work, we will consider the possibility of partial network perturbation for neural networks other than the autoencoder, and achieve more efficient corresponding DP schemes.

References

1. Abadi, M., Chu, A., Goodfellow, I., McMahan, H.B., Mironov, I., Talwar, K., Zhang, L.: Deep learning with differential privacy. In: Proceedings of the 2016 ACM SIGSAC conference on computer and communications security. pp. 308–318 (2016)
2. Bagdasaryan, E., Poursaeed, O., Shmatikov, V.: Differential privacy has disparate impact on model accuracy. *Advances in neural information processing systems* **32** (2019)
3. Balle, B., Barthe, G., Gaboardi, M., Hsu, J., Sato, T.: Hypothesis testing interpretations and renyi differential privacy. In: International Conference on Artificial Intelligence and Statistics. pp. 2496–2506. PMLR (2020)

4. Becht, E., McInnes, L., Healy, J., Dutertre, C.A., Kwok, I.W., Ng, L.G., Ginhoux, F., Newell, E.W.: Dimensionality reduction for visualizing single-cell data using umap. *Nature biotechnology* **37**(1), 38–44 (2019)
5. Biase, F.H., Cao, X., Zhong, S.: Cell fate inclination within 2-cell and 4-cell mouse embryos revealed by single-cell rna sequencing. *Genome research* **24**(11), 1787–1796 (2014)
6. Bonomi, L., Huang, Y., Ohno-Machado, L.: Privacy challenges and research opportunities for genomic data sharing. *Nature genetics* **52**(7), 646–654 (2020)
7. Chen, J., Wang, W.H., Shi, X.: Differential privacy protection against membership inference attack on machine learning for genomic data. In: *BIOCOMPUTING 2021: Proceedings of the Pacific Symposium*. pp. 26–37. World Scientific (2020)
8. Chen, L., He, Q., Zhai, Y., Deng, M.: Single-cell rna-seq data semi-supervised clustering and annotation via structural regularized domain adaptation. *Bioinformatics* **37**(6), 775–784 (2021)
9. Chen, X., He, K.: Exploring simple siamese representation learning. In: *Proceedings of the IEEE/CVF conference on computer vision and pattern recognition*. pp. 15750–15758 (2021)
10. Dwork, C.: A firm foundation for private data analysis. *Communications of the ACM* **54**(1), 86–95 (2011)
11. Dwork, C., McSherry, F., Nissim, K., Smith, A.: Calibrating noise to sensitivity in private data analysis. In: *Theory of Cryptography: Third Theory of Cryptography Conference, TCC 2006, New York, NY, USA, March 4-7, 2006. Proceedings 3*. pp. 265–284. Springer (2006)
12. Dwork, C., Roth, A., et al.: The algorithmic foundations of differential privacy. *Foundations and Trends® in Theoretical Computer Science* **9**(3–4), 211–407 (2014)
13. Eraslan, G., Simon, L.M., Mircea, M., Mueller, N.S., Theis, F.J.: Single-cell rna-seq denoising using a deep count autoencoder. *Nature communications* **10**(1), 390 (2019)
14. Flores, M., Liu, Z., Zhang, T., Hasib, M.M., Chiu, Y.C., Ye, Z., Paniagua, K., Jo, S., Zhang, J., Gao, S.J., et al.: Deep learning tackles single-cell analysis—a survey of deep learning for scrna-seq analysis. *Briefings in bioinformatics* **23**(1), bbab531 (2022)
15. Fu, J., Chen, Z., Han, X.: Adap dp-fl: Differentially private federated learning with adaptive noise. In: *2022 IEEE International Conference on Trust, Security and Privacy in Computing and Communications (TrustCom)*. pp. 656–663. IEEE (2022)
16. Fu, J., Ye, Q., Hu, H., Chen, Z., Wang, L., Wang, K., Xun, R.: Dpsur: Accelerating differentially private stochastic gradient descent using selective update and release. *arXiv preprint arXiv:2311.14056* (2023)
17. Grønbech, C.H., Vording, M.F., Timshel, P.N., Sønderby, C.K., Pers, T.H., Winther, O.: scvae: variational auto-encoders for single-cell gene expression data. *Bioinformatics* **36**(16), 4415–4422 (2020)
18. Ha, T., Dang, T.K., Dang, T.T., Truong, T.A., Nguyen, M.T.: Differential privacy in deep learning: an overview. In: *2019 International Conference on Advanced Computing and Applications (ACOMP)*. pp. 97–102. IEEE (2019)
19. Houssiau, F., Rocher, L., de Montjoye, Y.A.: On the difficulty of achieving differential privacy in practice: user-level guarantees in aggregate location data. *Nature communications* **13**(1), 29 (2022)
20. Hubert, L., Arabie, P.: Comparing partitions. *Journal of classification* **2**, 193–218 (1985)

21. Islam, M.M., Mohammed, N., Wang, Y., Hu, P.: Differential private deep learning models for analyzing breast cancer omics data. *Frontiers in oncology* **12**, 879607 (2022)
22. Klein, A.M., Mazutis, L., Akartuna, I., Tallapragada, N., Veres, A., Li, V., Peshkin, L., Weitz, D.A., Kirschner, M.W.: Droplet barcoding for single-cell transcriptomics applied to embryonic stem cells. *Cell* **161**(5), 1187–1201 (2015)
23. Kullback, S., Leibler, R.A.: On information and sufficiency. *The annals of mathematical statistics* **22**(1), 79–86 (1951)
24. Leemann, T., Pawelczyk, M., Kasneci, G.: Gaussian membership inference privacy. *Advances in Neural Information Processing Systems* **36** (2024)
25. Li, H., Courtois, E.T., Sengupta, D., Tan, Y., Chen, K.H., Goh, J.J.L., Kong, S.L., Chua, C., Hon, L.K., Tan, W.S., et al.: Reference component analysis of single-cell transcriptomes elucidates cellular heterogeneity in human colorectal tumors. *Nature genetics* **49**(5), 708–718 (2017)
26. Liu, H., Wu, Z., Peng, C., Lei, X., Tian, F., Lu, L.: Adaptive differential privacy of character and its application for genome data sharing. In: 2019 International Conference on Networking and Network Applications (NaNA). pp. 429–436. IEEE (2019)
27. Mironov, I.: Rényi differential privacy. In: 2017 IEEE 30th computer security foundations symposium (CSF). pp. 263–275. IEEE (2017)
28. Mironov, I., Talwar, K., Zhang, L.: Rényi differential privacy of the sampled gaussian mechanism. *arXiv preprint arXiv:1908.10530* (2019)
29. Muraro, M.J., Dharmadhikari, G., Grün, D., Groen, N., Dielen, T., Jansen, E., Van Gorp, L., Engelse, M.A., Carlotti, F., De Koning, E.J., et al.: A single-cell transcriptome atlas of the human pancreas. *Cell systems* **3**(4), 385–394 (2016)
30. Ocasio, J.K., Babcock, B., Malawsky, D., Weir, S.J., Loo, L., Simon, J.M., Zylka, M.J., Hwang, D., Dismuke, T., Sokolsky, M., et al.: scRNA-seq in medulloblastoma shows cellular heterogeneity and lineage expansion support resistance to shh inhibitor therapy. *Nature communications* **10**(1), 5829 (2019)
31. Oestreich, M., Chen, D., Schultze, J.L., Fritz, M., Becker, M.: Privacy considerations for sharing genomics data. *EXCLI journal* **20**, 1243 (2021)
32. Papernot, N., Song, S., Mironov, I., Raghunathan, A., Talwar, K., Erlingsson, Ú.: Scalable private learning with pate. *arXiv preprint arXiv:1802.08908* (2018)
33. Romanov, R.A., Zeisel, A., Bakker, J., Girach, F., Helysaz, A., Tomer, R., Alpar, A., Mulder, J., Clotman, F., Keimpema, E., et al.: Molecular interrogation of hypothalamic organization reveals distinct dopamine neuronal subtypes. *Nature neuroscience* **20**(2), 176–188 (2017)
34. Rumelhart, D.E., Hinton, G.E., Williams, R.J.: Learning representations by back-propagating errors. *nature* **323**(6088), 533–536 (1986)
35. Shen, Y., Wang, Z., Sun, R., Shen, X.: Towards understanding the impact of model size on differential private classification. *arXiv preprint arXiv:2111.13895* (2021)
36. Strehl, A., Ghosh, J.: Cluster ensembles—a knowledge reuse framework for combining multiple partitions. *Journal of machine learning research* **3**(Dec), 583–617 (2002)
37. Tian, T., Wan, J., Song, Q., Wei, Z.: Clustering single-cell rna-seq data with a model-based deep learning approach. *Nature Machine Intelligence* **1**(4), 191–198 (2019)
38. Tian, T., Zhang, J., Lin, X., Wei, Z., Hakonarson, H.: Model-based deep embedding for constrained clustering analysis of single cell rna-seq data. *Nature communications* **12**(1), 1873 (2021)

39. Tramèr, F., Huang, Z., Hubaux, J.P., Ayday, E.: Differential privacy with bounded priors: reconciling utility and privacy in genome-wide association studies. In: Proceedings of the 22nd ACM SIGSAC Conference on Computer and Communications Security. pp. 1286–1297 (2015)
40. Wang, J., Xia, J., Wang, H., Su, Y., Zheng, C.H.: scdcca: deep contrastive clustering for single-cell rna-seq data based on auto-encoder network. *Briefings in Bioinformatics* **24**(1), bbac625 (2023)
41. Wang, J., Ma, A., Chang, Y., Gong, J., Jiang, Y., Qi, R., Wang, C., Fu, H., Ma, Q., Xu, D.: scgcn is a novel graph neural network framework for single-cell rna-seq analyses. *Nature communications* **12**(1), 1882 (2021)
42. Wu, X., Wei, Y., Mao, Y., Wang, L.: A differential privacy dna motif finding method based on closed frequent patterns. *Cluster computing* **22**(Suppl 2), 2907–2919 (2019)
43. Xia, T., Shen, S., Yao, S., Fu, X., Xu, K., Xu, X., Fu, X.: Differentially private learning with per-sample adaptive clipping. In: Proceedings of the AAAI Conference on Artificial Intelligence. vol. 37, pp. 10444–10452 (2023)
44. Yan, J., Ma, M., Yu, Z.: bmvae: a variational autoencoder method for clustering single-cell mutation data. *Bioinformatics* **39**(1), btac790 (2023)
45. Yan, L., Yang, M., Guo, H., Yang, L., Wu, J., Li, R., Liu, P., Lian, Y., Zheng, X., Yan, J., et al.: Single-cell rna-seq profiling of human preimplantation embryos and embryonic stem cells. *Nature structural & molecular biology* **20**(9), 1131–1139 (2013)
46. Ye, D., Shen, S., Zhu, T., Liu, B., Zhou, W.: One parameter defense—defending against data inference attacks via differential privacy. *IEEE Transactions on Information Forensics and Security* **17**, 1466–1480 (2022)
47. Yilmaz, E., Ji, T., Ayday, E., Li, P.: Genomic data sharing under dependent local differential privacy. In: Proceedings of the twelfth ACM conference on data and application security and privacy. pp. 77–88 (2022)
48. Yu, Z., Lu, Y., Wang, Y., Tang, F., Wong, K.C., Li, X.: Zinb-based graph embedding autoencoder for single-cell rna-seq interpretations. In: Proceedings of the AAAI conference on artificial intelligence. vol. 36, pp. 4671–4679 (2022)
49. Yu, Z., Su, Y., Lu, Y., Yang, Y., Wang, F., Zhang, S., Chang, Y., Wong, K.C., Li, X.: Topological identification and interpretation for single-cell gene regulation elucidation across multiple platforms using scmgca. *Nature Communications* **14**(1), 400 (2023)
50. Zeisel, A., Muñoz-Manchado, A.B., Codeluppi, S., Lönnerberg, P., La Manno, G., Juréus, A., Marques, S., Munguba, H., He, L., Betsholtz, C., et al.: Cell types in the mouse cortex and hippocampus revealed by single-cell rna-seq. *Science* **347**(6226), 1138–1142 (2015)
51. Zheng, G.X., Terry, J.M., Belgrader, P., Ryvkin, P., Bent, Z.W., Wilson, R., Zalando, S.B., Wheeler, T.D., McDermott, G.P., Zhu, J., et al.: Massively parallel digital transcriptional profiling of single cells. *Nature communications* **8**(1), 14049 (2017)
52. Zhu, K., Van Hentenryck, P., Fioretto, F.: Bias and variance of post-processing in differential privacy. In: Proceedings of the AAAI Conference on Artificial Intelligence. vol. 35, pp. 11177–11184 (2021)
53. Zhu, T., Li, G., Zhou, W., Philip, S.Y.: Differential privacy and applications. Springer (2017)